Lawrence Berkeley National Laboratory

Lawrence Berkeley National Laboratory

Title

Structure, Magnetism, and Transport of CuCr2Se4 Thin Films

Permalink

https://escholarship.org/uc/item/7cf7f723

Authors

Bettinger, J.S.
Chopdekar, R.V.
Liberati, M.
et al.

Publication Date

2008-06-24

eScholarship.org Powered by the California Digital Library
University of California

Structure, Magnetism, and Transport of $CuCr_2Se_4$ Thin Films

J.S. Bettinger[1], R.V. Chopdekar[1,2], M. Liberati[3,4], J.R. Neulinger[5], M. Chshiev[6], Y. Takamura[1], L.M.B. Alldredge[1,2], E. Arenholz[4], Y.U. Idzerda[3], A.M. Stacy[5], W.H. Butler[6,7,] Y. Suzuki[1]

[1]Department of Materials Science and Engineering, UC Berkeley, Berkeley, California;

[2]School of Applied Physics, Cornell University, Ithaca, New York;

[3]Department of Physics, Montana State University, Bozeman, Montana;

[4]Advanced Light Source, Lawrence Berkeley National Laboratory, Berkeley, California;

[5]Department of Chemistry, UC Berkeley, Berkeley, California;

[6]MINT Center, University of Alabama, Tuscaloosa, Alabama;

[7]Department of Physics and Astronomy, University of Alabama, Tuscaloosa, Alabama.

ABSTRACT

We report the successful growth of highly spin-polarized chalcogenide thin films of $CuCr_2Se_4$, which are promising candidates for spin-based electronic applications. We also present electronic structure calculations for $CuCr_2Se_4$ that, together with magnetic and transport data, imply that the stoichiometric compound is a metallic ferromagnet with a relatively low density of hole-like carriers at the Fermi energy. These calculations also predict that a deficiency of Se will deplete the minority density of states at the Fermi energy perhaps leading to a half-metal. We have successfully grown thin films of $CuCr_2Se_4$ by pulsed laser deposition on isostructural $MgAl_2O_4$ substrates followed by an anneal in a Se-rich environment. X-ray diffraction confirms the structure of $CuCr_2Se_4$ on $MgAl_2O_4$ substrates as well as a secondary phase of Cr_2Se_3. X-ray absorption spectroscopy indicates that the chemical structure at the surface of the films is similar to that of bulk $CuCr_2Se_4$ single crystals. Magnetization measurements indicate that these films saturate with a magnetic moment close to 5 μ_B per formula unit and a T_c above 400 K. X-ray magnetic circular dichroism shows that the magnetism persists to the surface of the film. Resistivity and Hall effect measurements are consistent with a p-type ferromagnetic metallic behavior and with the electronic structure calculations.

1. Introduction

Recently, there has been an enormous amount of research on the development of highly spin-polarized materials in light of their potential incorporation into spin-based electronic applications. However, there remain fundamental questions associated with highly spin polarized materials such as the nature of magnetism at surfaces and interfaces. Many of these materials studies have been focused on binary and ternary oxides, including CrO_2, Fe_3O_4, $La_{0.7}Sr_{0.3}MnO_3$, and $SrFeMoO_6$.[1] They have been successfully synthesized in thin film form and incorporated into prototypical spin-based devices.

While complex oxide materials have been well studied to this end, complex chalcogenides have not been explored for magnetic devices. Of particular interest is the family of chalcogenide spinels, AB_2X_4, where X is one of S, Se, or Te. In contrast to the oxide spinels, one may hope that the decrease in the ionic character of the bonds in the chalcogenides may lead to transport properties more similar to ordinary metals and semiconductors. The bulk properties of most chalcogenide spinels were examined in the 1960s. They exhibit a wide range of electronic and magnetic behavior.[2-6] Within the family of chalcogenide spinels, the basic structural parameters, such as the S-S or Se-Se distances, as well as thermal properties such as thermal expansion are very similar for most members of the family, so *epitaxial growth* of thin isostructural layers is generally possible. Therefore, one can imagine synthesizing and fabricating an all-chalcogenide spinel multilayer magnetic device. More recently these materials have been the objects of renewed study as high magnetoresistance materials.[7]

Of the many known chalcogenide spinel materials, $CuCr_2Se_4$ is a promising candidate for magnetic devices. It is a ferromagnetic metallic material that has been synthesized in bulk form since the 1960s but has yet to be grown in thin film form.[5] Bulk forms of $CuCr_2Se_4$ have

magnetization near 5 μ_B per formula unit at low temperatures and have a relatively high Curie temperature (T_C) of 444 K.[8] The crystal structure is a normal spinel, made of an fcc lattice of Se with Cu cations in 1/8 of the tetrahedral sites and Cr cations in 1/2 of the octahedral sites. Bulk studies indicate that deviations from stoichiometry can give rise to poorer metallic conductivity and even semiconducting behavior.[9]

2. Electronic Structure Calculations

The calculated electronic structure of $CuCr_2Se_4$ is shown in Figures (1-3). The calculations were performed using the Generalized Gradient Approximation (GGA) within Density Functional Theory (DFT). The Vienna ab-initio simulation program (VASP) [10-15] implementation of DFT using Projector Augmented Waves was employed for the calculations. The calculations shown here are based on a fully relaxed structure (a=10.395 Å, u=0.00767) but differed only slightly from those based on the experimental structure (a=10.334 Å, u=0.00739). The spin-orbit interaction was not included in the calculations and possible orbital contributions to the magnetization were neglected.

Figure 1 shows the total density of states. Figure 2 shows the density of states decomposed by site and angular momentum component. The Se-p states are spread over a range of approximately 9 eV due to their hybridization with the Cr and Cu -d states. The Cr majority-d states hybridize with the Se-p states and spread from approximately 4 eV below the Fermi level to 2 eV above it. The Cr minority d-states are almost all above the Fermi-energy. The Se-p states are largely, but not completely filled. The Cu-d states also hybridize strongly with the Se-p states, but lie somewhat higher on average than the Cr-d states. The Cu-d states are filled except for a few unfilled majority states. The magnetic moment lies mainly on the Cr atoms which have

a moment of nearly 3 μ_B per ion and are aligned ferromagnetically. The Cr moments are partially compensated by small moments of opposite sign on the Cu and Se atoms so that the total calculated moment is slightly greater than 5 μ_B per formula unit (5.12 μ_B or 338 emu/cm^3). It should be noted that this picture is similar to that deduced from neutron diffraction studies in reference [3] and from XMCD in reference [16].

We also performed LDA+U calculations (not shown) in which a Coulomb U of 5 eV was applied to the d-states of the Cu and Cr ions. Interestingly, the electronic structure did not change qualitatively from the GGA result. The moment increased to 5.61 μ_B. Otherwise the electronic structure was qualitatively similar. We expect correlation effects to be less important in the chalcogenides than the oxides because of the more extended nature of the ligand wave functions. For $CuCr_2Se_4$, the fact that the system is basically ferromagnetic with a very delocalized anti-ferromagnetic component (spread over the Se and Cu ions) rather than a ferrimagnetic system like most magnetic spinels, probably helps to delocalize the electrons and reduce the correlation effects that cannot be treated by the mean-field DFT-GGA approach.

The unfilled energy bands for both the majority and minority spin channels near the Fermi energy indicate that $CuCr_2Se_4$ is predicted to be metallic. The Fermi surface (Fig. 3) is relatively simple for the minority channel which has three closed hole surfaces centered at the Γ-point. These three surfaces have relatively high dispersion as evidenced by the low and smooth density of states in the minority channel at the Fermi energy. We estimate based on the calculated integrated DOS that these three surfaces contain 0.065 holes per formula unit. The smallest hole surface has a Fermi velocity of 5.5 x 10^5 m/sec and an effective mass of 0.26 m_e in the Γ-X direction. In this direction, the larger hole surfaces have a Fermi velocity of approximately 3.5x10^5 m/sec and a mass of 0.65 m_e. We emphasize that the conduction electrons

in this material differ qualitatively from the massive, low velocity electrons commonly encountered in transition metal oxides. Our calculated electronic structure in the vicinity of the Fermi energy is similar to that obtained by Ogata et al. [17] using the DV-Xα method. Relativistic calculations [18] however, do not show the smallest minority hole surface because of a splitting which leaves the Γ point just above the Fermi energy doubly rather than triply degenerate.

The majority bands that cross the Fermi energy consist of a single highly dispersive band that forms a closed hole surface surrounding the Γ-point, and two additional, less dispersive bands that are degenerate along Γ-X and Γ-L. These two bands give the structure in the majority DOS that extends from just below the Fermi surface to a narrow gap in the majority DOS that begins approximately 0.2 eV above E_F. We estimate that the closed hole surface contains approximately 0.02 electrons per formula unit. The electrical conductivity will depend not only on the number and velocities of the carriers but also on the scattering mechanisms which will depend on the temperature and on the concentration and types of defects. However, based on the Fermi surface alone, we would expect the current to be carried primarily by down-spin holes, thus making it a candidate for highly spin polarized electrodes for magnetic tunnel junctions. The reason for this is that there are more minority holes than majority holes (not counting the less dispersive bands) and the much higher density of states for majority than for minority is expected to increase the scattering rate for majority. An additional reason that we expect higher conductance from the minority bands is the absence of localized Cr-d states near the Fermi energy for the minority channel. The minority states near the Fermi energy seem to be quite delocalized, having contributions from all of the ions in the cell. Our picture of delocalized electrons at the Fermi energy seems to be consistent with the measured resistivity [9] which is

reported to be as low as 25 μΩcm at low temperature, rising to approximately 300 μΩcm at room temperature. Thus $CuCr_2Se_4$ is a surprisingly good metal for a transition metal based material with such a large unit cell.

An estimate of the carrier density based on the estimated volumes of the closed hole surfaces yields 4.1 x $10^{20}/cm^3$ for the minority hole surfaces and $1.4x10^{20}/cm^3$ for the majority closed hole surface. In addition, there are two majority open surfaces for which the designation hole or electron is ambiguous but which are likely to have larger regions with negative curvature (holes) than positive. We have not attempted a rigorous calculation of the low field hall constant, which would require an average over the Fermi surface of the mean curvature weighted by the square of the electron velocity.[19-21] The experimental value of the Hall carrier density, n_H, obtained by the extrapolation of measurements on $CuCr2Se_{4-x}Br_x$ to x=0 [9], is consistent with hole conduction, but is an order of magnitude greater than our estimate of the carrier density based on the closed surfaces only. It should be emphasized, however, that the Hall carrier density, $n_H=-1/(R_Hec)$ is only equal to the number of carriers for spherical Fermi surfaces.

3. $CuCr_2Se_4$ Thin Films

In the context of the calculated electronic structure, we present our study on the successful growth of crystalline magnetic thin films of $CuCr_2Se_4$ via a two step process, first using pulsed laser deposition (PLD) to grow stoichiometric films, and then performing an anneal in a Se-rich environment to promote the correct phase of $CuCr_2Se_4$. X-ray diffraction, as well as magnetic and electronic transport characterization, indicates that as-grown films are a combination of $CuCrSe_2$ and ferrimagnetic $Cr_{3-x}Se_4$. Following the Se-rich anneal, we can successfully synthesize metallic ferrimagnetic $CuCr_2Se_4$ films. Soft X-ray absorption

spectroscopy (XAS) indicates that the chemical structure at the surface of the films is similar to that of bulk $CuCr_2Se_4$. Bulk magnetic measurements indicate that these films saturate with a magnetic moment close to 5 μ_B per formula unit and have a T_c above 400 K. X-ray magnetic circular dichroism (XMCD) measurements, which probe about 5-10 nm into the sample, reveal strong circular dichroism in the post-annealed films, thus suggesting that the magnetic properties of the $CuCr_2Se_4$ persist to the surface and would thus be suitable for spin-based devices. Resistivity and Hall effect measurements are consistent with p-type ferromagnetic metallic behavior.

(a) Thin Film Synthesis

We have synthesized these chalcogenide films by PLD followed by a post-deposition annealing step in a vacuum-sealed quartz tube with a Se source. For PLD, sintered ceramic targets of $CuCr_2Se_4$ were pressed from hand-ground $CuCr_{2.003}Se_{4.089}$ powder. The powder was prepared by mixing the elements in a vacuum-sealed quartz tube and heating to 800 ºC for 7 days. This was then pressed into a target with a 0.5 inch inner diameter stainless steel die at room temperature to a pressure of 2500 lbs with a hydraulic laboratory press. The pellet was then sintered for 22 hours at 1150 ºC in an evacuated quartz tube. We have determined that optimal thin film growth occurs in vacuum (base pressure of 1 x 10^{-6} Torr) at 600 °C-650 °C on an isostructural substrate of (100) $MgAl_2O_4$. The KrF excimer laser (248 nm) was operated at 3 Hz and a fluence of 5-6 J/cm^2. Post-deposition annealing *ex-situ* in vacuum-sealed quartz tubes with Se for 48 hours at 475 °C promotes the growth of the spinel $CuCr_2Se_4$. This two-step process has enabled not only successful growth and characterization of $CuCr_2Se_4$, but also the investigation of other selenides which have not previously been studied in thin film form.

(b) Structure

The structure of our films has been characterized through X-ray diffraction. In as-deposited films (Fig. 4a), we see reflections at 2θ values of 27.72° and 30.68°, corresponding to the $CuCrSe_2$ {0 0 6} and $Cr_{2.8}Se_4$ {4 0 0} planes. We also see higher order reflections at 2θ values of 57.12° and 63.80°, corresponding to the $CuCrSe_2$ {0 0 12} and $Cr_{2.8}Se_4$ {8 0 0} planes. Both crystal structures are similar to the spinel $CuCr_2Se_4$. $CuCrSe_2$ is made of an fcc lattice of Se with Cr in ½ of the octahedral voids making $CrSe_2$ sandwiches, and Cu in ½ of the tetrahedral voids between these sandwiches.[22,23] $Cr_{3-\delta}Se_4$ is an off-stoichiometric version of Cr_3Se_4 [24] which has a NiAs-like structure. Here, the Se anions make an hcp lattice with Cr in ¾ of the octahedral voids. $Cr_{3-\delta}Se_4$ is missing some of the Cr cations in the stoichiometric structure. After the Se anneal (Fig. 4b), we observe the reflections corresponding to the $CuCr_2Se_4$ {111} lattice planes. Additional reflections in the diffraction pattern are most likely attributed to Cr_2Se_3, an antiferromagnetic material with a Neel temperature (T_N) of 45 K.[25] From Rutherford backscattering spectroscopy, we routinely find Cu deficiency in our films. This finding is consistent with the synthesis of Cr_2Se_3 along with $CuCr_2Se_4$ in the post-annealed films.

Through our two-step process, we have grown two different magnetic chalcogenides, $CuCr_2Se_4$ and $Cr_{3-\delta}Se_4$. $CuCr_2Se_4$ is a highly spin-polarized spinel that has a T_c of 444 K. The magnetic moment comes from the occupation of the majority Cr d-states, but not the minority as described above. $Cr_{3-\delta}Se_4$ is an off-stoichiometric form of Cr_3Se_4. By changing the Cr content, it is possible to obtain an antiferromagnet or a ferrimagnet.[24] $Cr_{3+\delta}Se_4$ ($0 \leq \delta \leq 0.2$) is an antiferromagnet with T_N of 88K for $\delta=0$ and a decreasing T_N for increasing Cr content. $Cr_{3-\delta}Se_4$

($0 < \delta \leq 0.2$), such as $Cr_{2.8}Se_4$ or $Cr_{2.9}Se_4$, is a ferrimagnet with a T_c of 88 K. The magnetism here was suggested to be approximately 2 μ_B per formula unit.

(c) Magnetization

A Quantum Design superconducting quantum interference device (SQUID) magnetometer was used to apply a magnetic field in the film plane and measure the magnetization as a function of applied field for as-grown and post-annealed films (Fig. 5a). The magnetic properties of the as-grown films are dominated by ferrimagnetic $Cr_{2.8}Se_4$; $CuCrSe_2$ only contributes a weak paramagnetic signal. The as-grown films saturate at 84 emu/cm^3, and magnetization versus temperature measurements indicate a magnetic transition around 70K which is depressed from the bulk value of 88 K. Post-annealed films show saturation magnetization values of 293 emu/cm^3, or 4.4 μ_B per formula unit, comparable with bulk values of approximately 5 μ_B per formula unit for $CuCr_2Se_4$. After anneal (Fig. 5b), magnetization versus temperature shows a Brillouin-like dependence with a magnetic transition above 400 K- the temperature limit of the SQUID magnetometer. The Curie temperature (T_c) is estimated to be approximately 405-410 K from the temperature dependence of magnetization slightly below 400 K.

We have also probed the chemical and magnetic properties within 5-10 nm of the surface of the post-annealed films at a temperature of 14 K by X-ray absorption spectroscopy (XAS) and X-ray magnetic circular dichroism (XMCD) measurements using total electron yield detection in 30 degree grazing X-ray incidence at ALS beamline 4.0.2. For the XMCD measurement, an external field of 0.53 T was applied. XAS (Fig. 6a) indicates that the chemical composition at the surface of post-annealed films is similar to that of the bulk.[16] XMCD spectra of Cr indicate

magnetism persists to the surface of the post-annealed films (Fig. 6b). Moreover, the XMCD lineshape is characteristic of Cr in an octahedral environment and compares well to bulk data.[16]

(d) Transport

The electronic transport properties of these films have been studied by measuring resistivity as a function of temperature at different fields applied out of plane. Both as-grown and post-annealed films exhibit metallic behavior (Fig. 7). As-grown films exhibit a kink in the metallic behavior that is coincident with the Curie temperature of $Cr_{2.8}Se_4$. Such a kink is characteristic of ferromagnets at their T_c's and corresponds to the disappearance of scattering due to long-range spin disorder below T_c. The resistivity values of approximately $1.8x10^{-3}$ Ω-cm at 320 K and $1.4x10^{-3}$ Ω-cm at 10 K are those of a poor metal and all of these observations are consistent with bulk studies of $Cr_{2.8}Se_4$.[24] The transport properties of as-grown films are nearly identical to bulk $Cr_{2.8}Se_4$ measurements, suggesting that the transport is dominated by $Cr_{2.8}Se_4$ and not $CuCrSe_2$. In contrast, the post-annealed samples exhibit metallic behavior similar to bulk $CuCr_2Se_4$ with resistivity values from $5x10^{-4}$ Ω-cm at 400K to $2x10^{-4}$ Ω-cm at 5 K.[9] We also observe a flattening out of the resistivity curve at low temperatures. We fit the low temperature resistivity data to the Bloch-Gruneissen formula, $A + BT^n$, and found the coefficient n to be approximately 2.7, implying that the scattering is largely electron-electron and electron-magnon scattering. The relatively high resistivity together with a metal-like increase in the resistivity with temperature suggests a low carrier density.

We have also studied both the anomalous and ordinary Hall Effect as a function of temperature in post-annealed thin films in order to probe carrier concentration of $CuCr_2Se_4$ as

well as the effects of impurity scattering. Figure 8a shows both the anomalous and ordinary contributions to the Hall resistance at 5 K and 300 K. The ordinary contribution indicates that this material is a p-type metal with an average carrier concentration of about 3 x 10^{20} /cm^3 over the entire temperature range. The anomalous Hall effect (AHE) is examined by subtracting out the linear background representing the contribution of the ordinary Hall effect (Fig. 8b), and there is a crossover in the sign of the AHE resistivity at 287 K. Bulk crystal data [9] also indicates that $CuCr_2Se_4$ is a p-type metal but with a much higher carrier concentration. We acknowledge that the ordinary Hall effect is not a good measure of the actual carrier concentration for materials with complicated electronic structure. However, the differences in these values between bulk single crystal and their films need to be addressed. We attribute these differences to the effects of impurities due to the presence of Cr_2Se_3 and a Se deficiency. A reduction in carrier concentration is also found in single crystals of $CuCr_2Se_{4-x}Br_x$ where Br is introduced as a dopant on the Se site.[9] The anomalous contribution nearly saturates at temperatures below 100 K with a small decrease in magnitude at very low temperature, and decreases in magnitude as a function of increasing temperature above 100 K; the anomalous Hall signal eventually switches sign at higher temperatures as seen in Fig. 7c. We measured anomalous Hall coefficients, R_s, as a function of temperature (Fig. 8c) and found that the temperature dependence and magnitude of R_s is consistent with recent data of bulk $CuCr_2Se_{4-x}Br_x$ for small values of x. Therefore, impurity scattering in our films must be taken into consideration due to the presence of nonmagnetic Cr_2Se_3.

4. Se Vacancies in $CuCr_2Se_4$

In order to model the effect of Se vacancies in $CuCr_2Se_4$, we calculated the electronic structure of $Cu_2Cr_4Se_7$. One Se atom was removed from the 14 atom basis of the fcc spinel cell and the resulting structure was relaxed. The structural relaxation resulted in a cell with a small trigonal distortion and a 3.6% increase in volume. Just as in the stoichiometric spinel structure, each Se atom is surrounded by 1 Cu and 3 Cr ions. However, there are small changes in the nearest neighbor distances that generate three slightly different Se environments. One of the Cu atoms retains four Se neighbors while the other has only three. One of the Cr atoms retains six neighboring Se atoms while the other three have only five.

The density of states is shown in Figures 9 and 10. The most noticeable effect of the Se vacancy is that the Fermi energy falls in a gap for the minority implying that the substoichiometric material (at least in this ordered form) is a half-metal. The magnetic moment increases to 6 μ_B (382 emu/cm^3). Compared to the stoichiometric system, it appears that all of the ions, (except for one Se) have lost minority spins (or gained majority spins) .

The Cu-d states for the Cu atom adjacent to a Se vacancy rise by approximately 0.2 eV, there is a narrow peak in the majority just above the Fermi energy that arises from Cr-d states on Cr ions adjacent to the vacancy, and from Se-p states on Se ions that are adjacent to the 3 Cr, each of which lost a Se neighbor. For the minority channel, the vacancy causes the Se-p states to narrow slightly at the upper edge resulting in a gap at the Fermi energy.

The Fermi surface properties are strongly modified (Fig. 11). The three minority hole surfaces disappear. The closed majority hole surface also is also gone leaving only open majority surfaces at the Fermi energy. It is difficult to compare the calculations for the ordered Se-deficient material with the experimental measurements because the vacancies are presumably disordered and their concentration is not determined. However, the calculations do indicate that

Se vacancies will likely decrease the density of hole-like carriers. This is qualitatively consistent with our experimental result of n_H=3 x 10^{20}/cm^3 which is much lower than the reported bulk value of 7 x 10^{21}/cm^3.

5. Conclusions

In this work, we have demonstrated the successful synthesis of spin polarized thin films of $CuCr_2Se_4$. The structural, chemical, magnetic, and transport characterization confirm that we have been successful in $CuCr_2Se_4$ film growth. We have also confirmed that their magnetic properties persist to the surface. Electronic structure calculations indicate delocalized electrons at the Fermi energy and the possibility of half-metallic behavior for substoichiometric films. These films are promising candidates for future spin based electronic devices.

The authors thank Kin Man Yu for RBS characterization and Jennifer E. Johnson for fruitful discussions. This work was funded by the NIRT program of the National Science Foundation (#0303774). The Advanced Light Source is supported by the U.S. Department of Energy, Basic Energy Sciences, under contract No. DE-AC02-05CH11231. Work at UA was also supported by MRSEC grant DMR0213985 and by the INSIC EHDR Program.

Figure Captions:

Figure 1: Calculated density of electronic states for stoichiometric $CuCr_2Se_4$. Inset shows zoomed area around origin.

Figure 2: Site and angular-momentum decomposed density of electronic states (Cr d, Cu d and Se p) for $CuCr_2Se_4$.

Figure 3: Majority and minority energy bands near Fermi Energy (dashed line) along Γ-X, Γ-K and Γ-L directions.

Figure 4: X-ray diffraction peaks of (a) as deposited films of $CuCrSe_2$ and $Cr_{2.8}Se_4$ and (b) post-annealed films of the chalcogenide spinel $CuCr_2Se_4$ and Cr_2Se_3.

Figure 5: (a) Magnetization vs. field measurements for as-deposited films containing $Cr_{2.8}Se_4$ and post-annealed films of $CuCr_2Se_4$; (b) Magnetization vs. temperature of the post-annealed film of $CuCr_2Se_4$.

Figure 6: (a) XAS measurement of $CuCr_2Se_4$ showing a characteristic lineshape for Cr in an octahedral environment; (b) XMCD of $CuCr_2Se_4$ showing the persistence of magnetism to the surface of the film.

Figure 7: Resistivity vs. temperature transport data demonstrating the poor metallic behavior of as-grown $Cr_{2.8}Se_4$ films and metallic behavior of $CuCr_2Se_4$ films.

Figure 8: (a) Total Hall effect, containing both the ordinary and anomalous contributions to the Hall effect at 5K and 300K of $CuCr_2Se_4$ films; (b) anomalous contribution to the Hall effect from 5K through 350K of $CuCr_2Se_4$ films; (c) anomalous Hall coefficient, R_s, from 5K through 350K in $CuCr_2Se_4$ films.

Figure 9: Calculated density of electronic states for substoichiometric $CuCr_2Se_{3.5}$ with a Se vacancy. Inset shows zoomed area around origin.

Figure 10: Site and angular-momentum decomposed density of electronic states (Cr d, Cu d and Se p) for substoichiometric $CuCr_2Se_{3.5}$.

Figure 11: Majority and minority energy bands near Fermi Energy (dashed line) along Γ-X, Γ-K and Γ-L directions for substoichiometric $CuCr_2Se_{3.5}$.

REFERENCES

[1] J. M. D. Coey and C. L. Chien, Mrs Bulletin **28,** 720-724 (2003).
[2] P. F. Bongers, C. Haas, A. M. J. Vanrun, and G. Zanmarch, Journal of Applied Physics **40,** 958-963 (1969).
[3] C. Colominas, Physical Review **153,** 558-560 (1967).
[4] J. B. Goodenough, Solid State Communications **5,** 577-580 (1967).
[5] F. K. Lotgering, Solid State Communications **2,** 55-56 (1964).
[6] M. Robbins, H. W. Lehmann, and J. G. White, Journal of Physics and Chemistry of Solids **28,** 897-902 (1967).
[7] A. P. Ramirez, R. J. Cava, and J. Krajewski, Nature **386,** 156-159 (1997).
[8] J. R. Neulinger, (Unpublished).
[9] W. L. Lee, S. Watauchi, V. L. Miller, R. J. Cava, and N. P. Ong, Science **303,** 1647-1649 (2004).
[10] G. Kresse and J. Hafner, Physical Review B **47,** 558-561 (1993).
[11] G. Kresse and J. Hafner, Physical Review B **49,** 14251-14269 (1994).
[12] G. Kresse and J. Furthmuller, Computational Materials Science **6,** 15-50 (1996).
[13] G. Kresse and J. Furthmuller, Physical Review B **54,** 11169-11186 (1996).
[14] P. E. Blochl, Physical Review B **50,** 17953-17979 (1994).
[15] G. Kresse and D. Joubert, Physical Review B **59,** 1758-1775 (1999).
[16] A. Kimura, J. Matsuno, J. Okabayashi, A. Fujimori, T. Shishidou, E. Kulatov, and T. Kanomata, Physical Review B **63,** 224420 (2001).
[17] F. Ogata, T. Hamajima, T. Kambara, and K. Ichiro, Journal of Physics C-Solid State Physics **15,** 3483-3492 (1982).
[18] V. N. Antonov, V. P. Antropov, B. N. Harmon, A. N. Yaresko, and A. Y. Perlov, Physical Review B **59,** 14552-14560 (1999).
[19] W. H. Butler, Physical Review B **29,** 4224-4229 (1984).
[20] M. Tsuji, Journal of the Physical Society of Japan **13,** 818-827 (1958).
[21] M. Tsuji, Journal of the Physical Society of Japan **13,** 979-986 (1958).
[22] F. M. R. Engelsman, G. A. Wiegers, F. Jellinek, and B. Van Laar, Journal of Solid State Chemistry **6,** 574-582 (1973).
[23] P. F. Bongers, C. F. Van Bruggen, J. Koopstra, W. P. F. A. M. Omloo, G. A. Wiegers, and F. Jellinek, Journal of Physics and Chemistry of Solids **29,** 977-984 (1968).
[24] A. Maurer and G. Collin, Journal of Solid State Chemistry **34,** 23-30 (1980).
[25] M. Yuzuri, Journal of the Physical Society of Japan **35,** 1252-1252 (1973).

Figure 1:

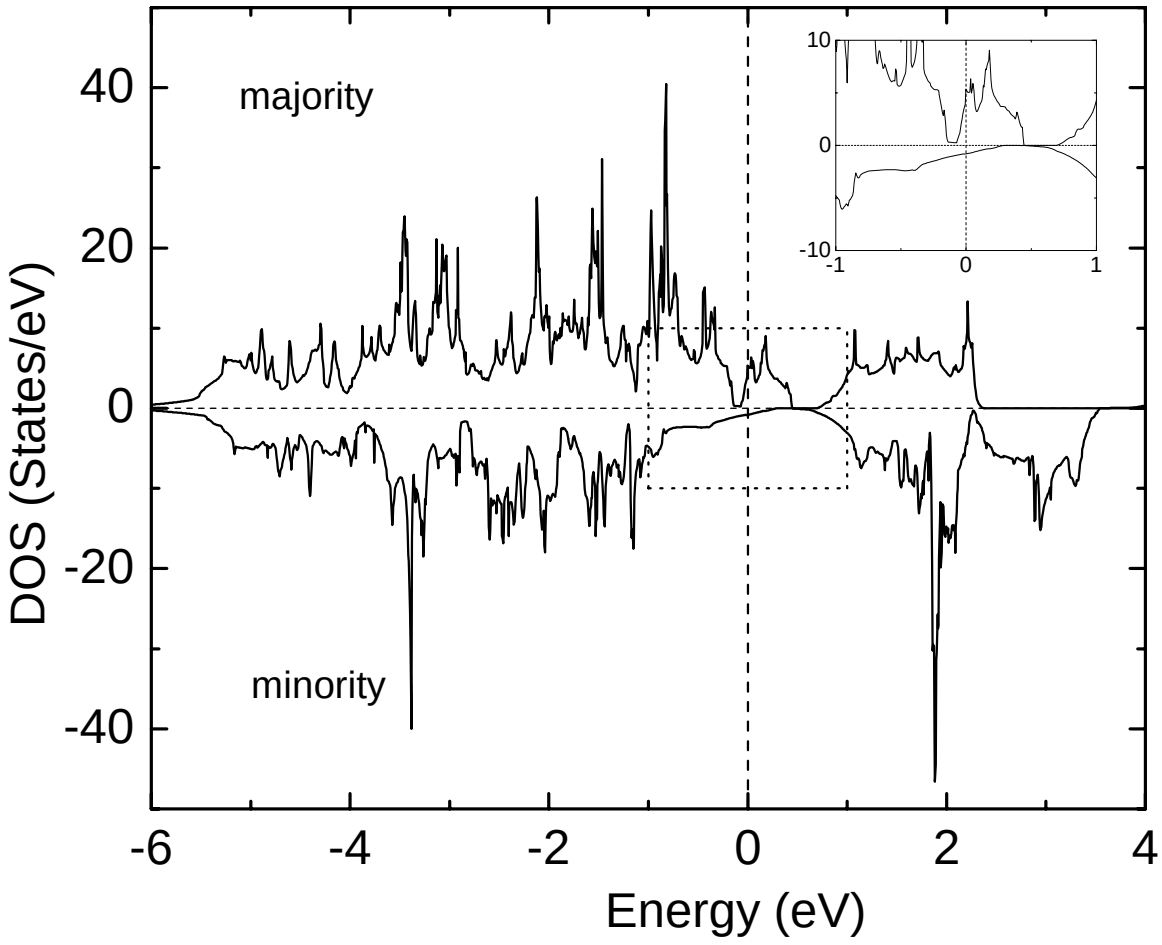
majority
minority
DOS (States/eV)
Energy (eV)
40
20
0
-20
-40
-6
-4
-2
0
2
4
10
0
-10
-1
0
1

Figure 2:

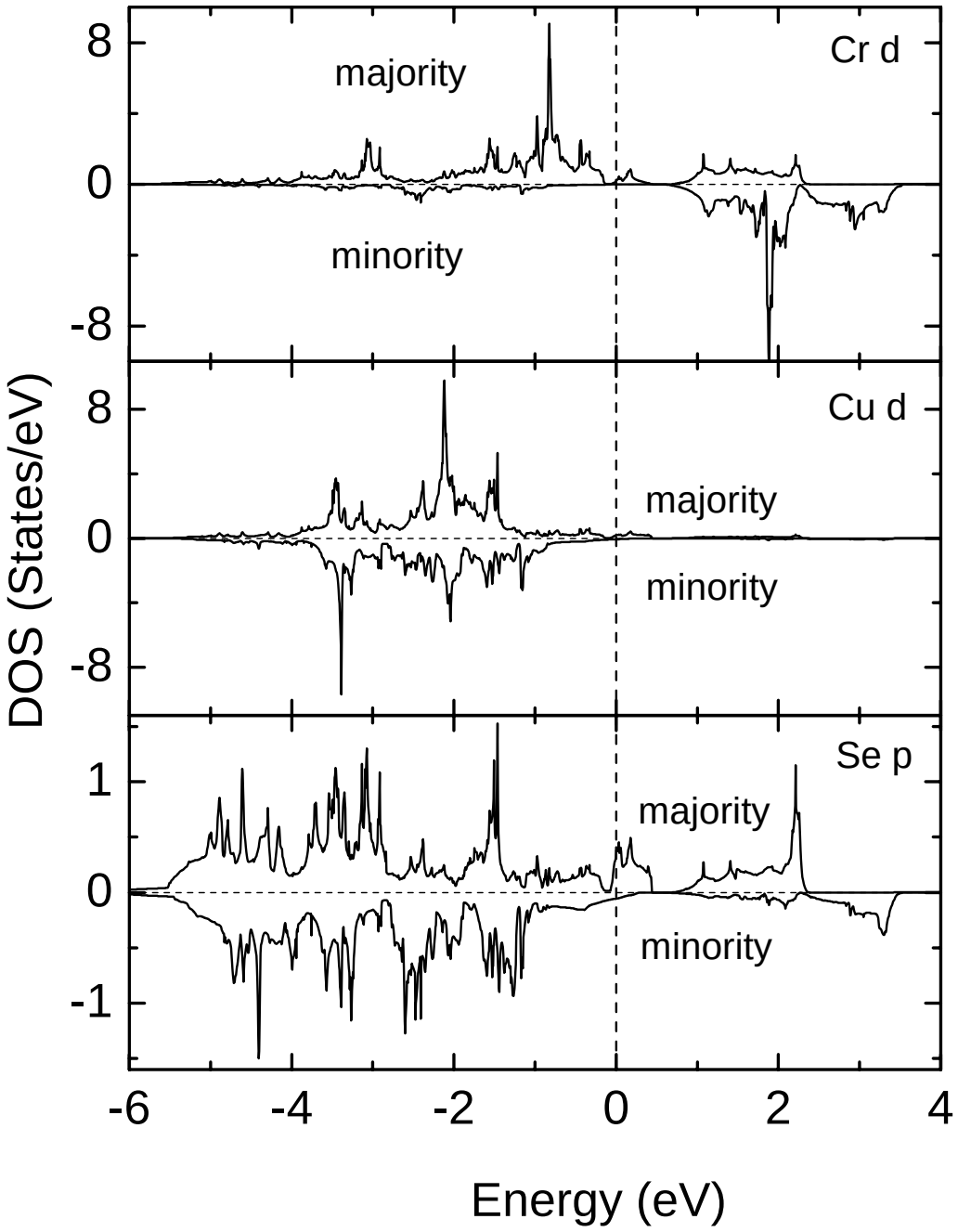
Cr d
majority
minority
Cu d
majority
minority
Se p
majority
minority
DOS (States/eV)
Energy (eV)
8
0
-8
8
0
-8
1
0
-1
-6
-4
-2
0
2
4

Figure 3:

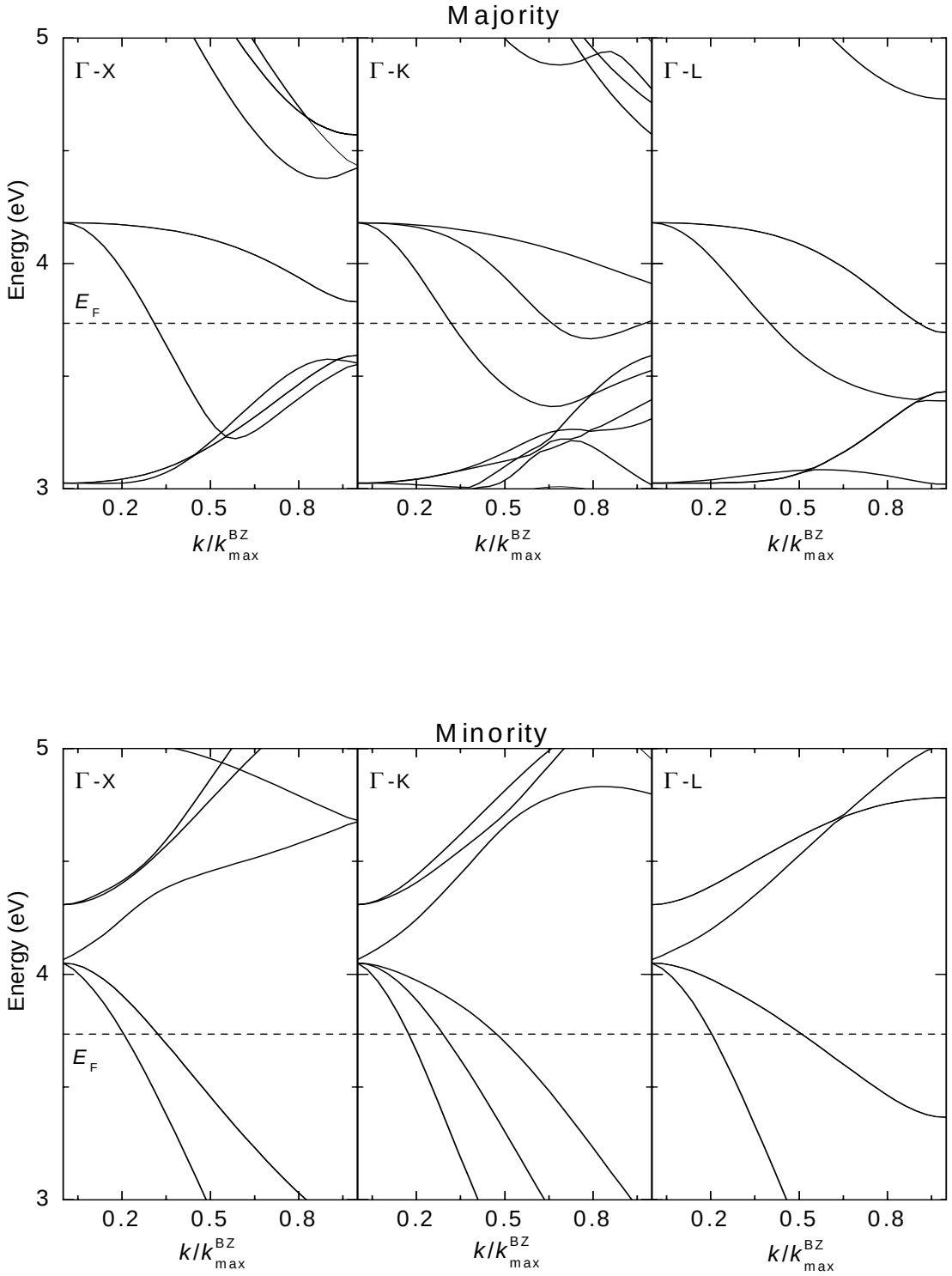
Majority
Γ-X
Γ-K
Γ-L
Energy (eV)
5
4
3
E_F
0.2
0.5
0.8
k/k^{BZ}_{max}
Minority
Γ-X
Γ-K
Γ-L
Energy (eV)
5
4
3
E_F
0.2
0.5
0.8
k/k^{BZ}_{max}

Figure 4:

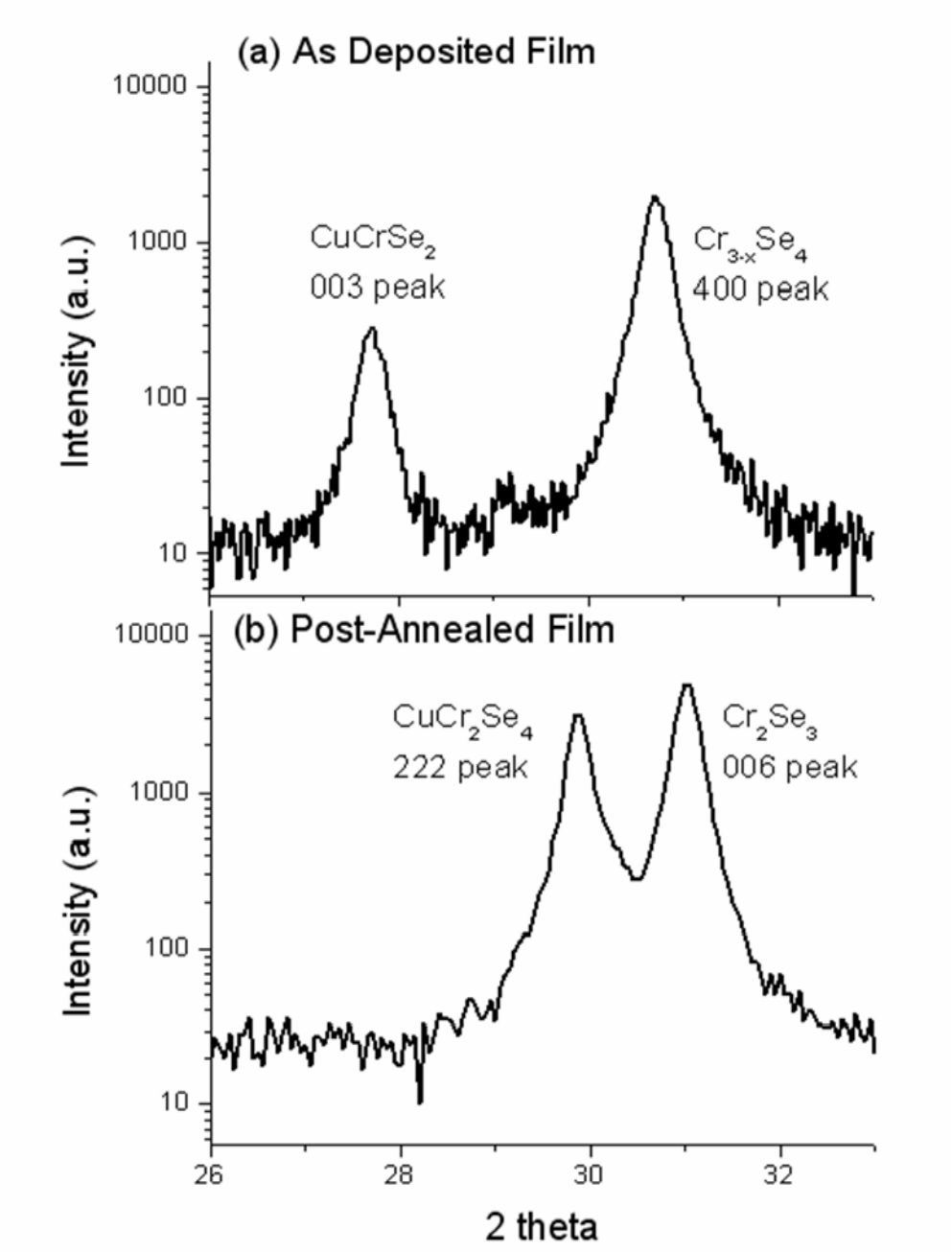
(a) As Deposited Film
10000
1000
100
10
Intensity (a.u.)
CuCrSe2
003 peak
Cr3-xSe4
400 peak
(b) Post-Annealed Film
10000
1000
100
10
Intensity (a.u.)
CuCr2Se4
222 peak
Cr2Se3
006 peak
26
28
30
32
2 theta

Figure 5:

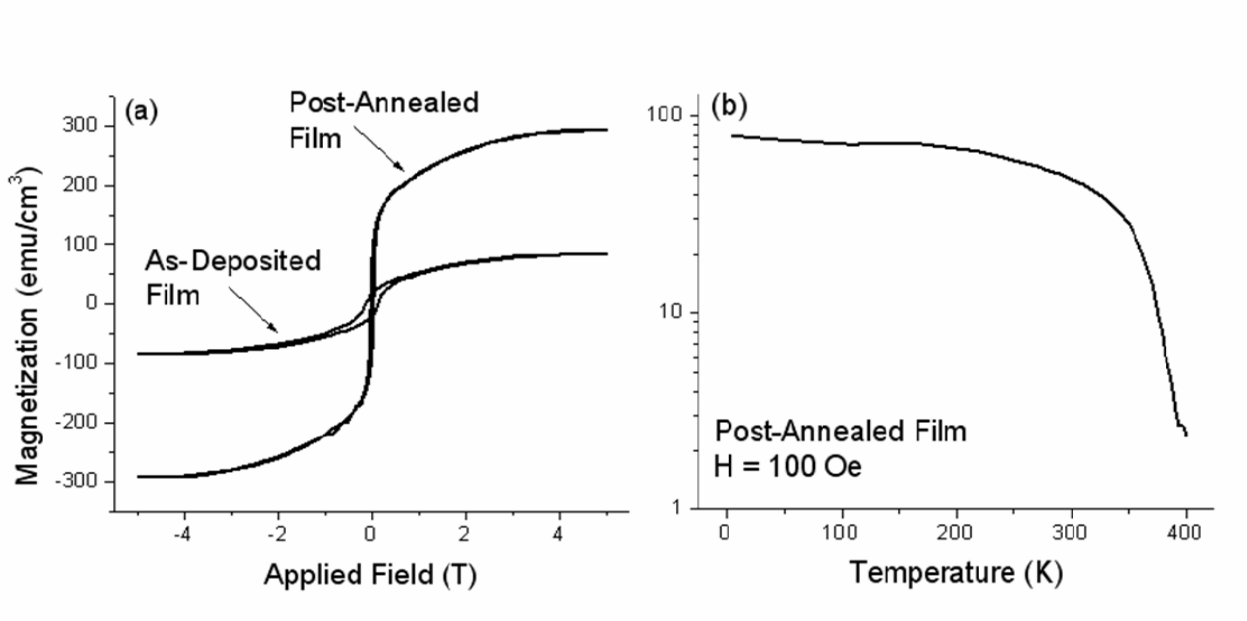
(a)
Post-Annealed Film
As-Deposited Film
Magnetization (emu/cm3)
300
200
100
0
-100
-200
-300
-4
-2
0
2
4
Applied Field (T)
(b)
100
10
1
Post-Annealed Film
H = 100 Oe
0
100
200
300
400
Temperature (K)

Figure 6:

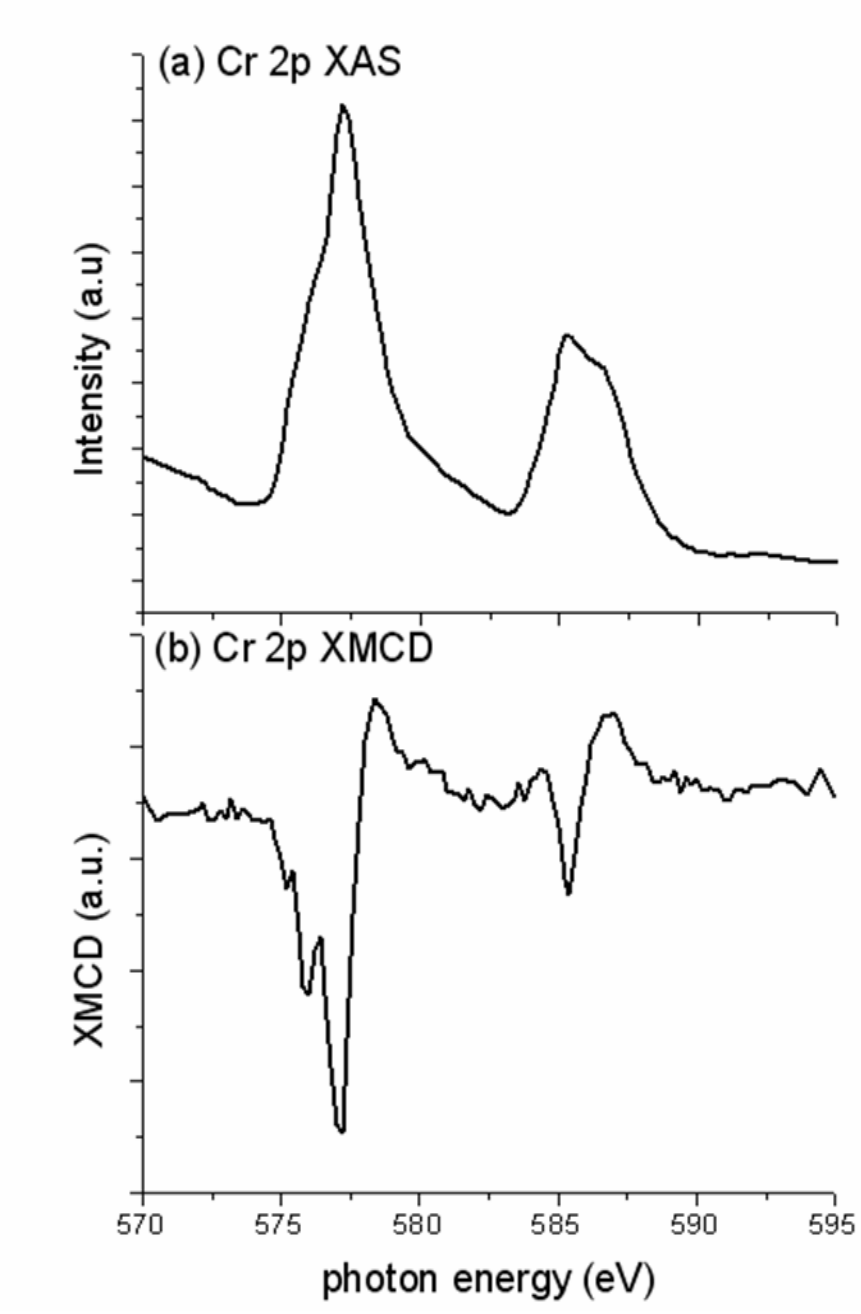
(a) Cr 2p XAS
Intensity (a.u)
(b) Cr 2p XMCD
XMCD (a.u.)
570
575
580
585
590
595
photon energy (eV)

Figure 7:

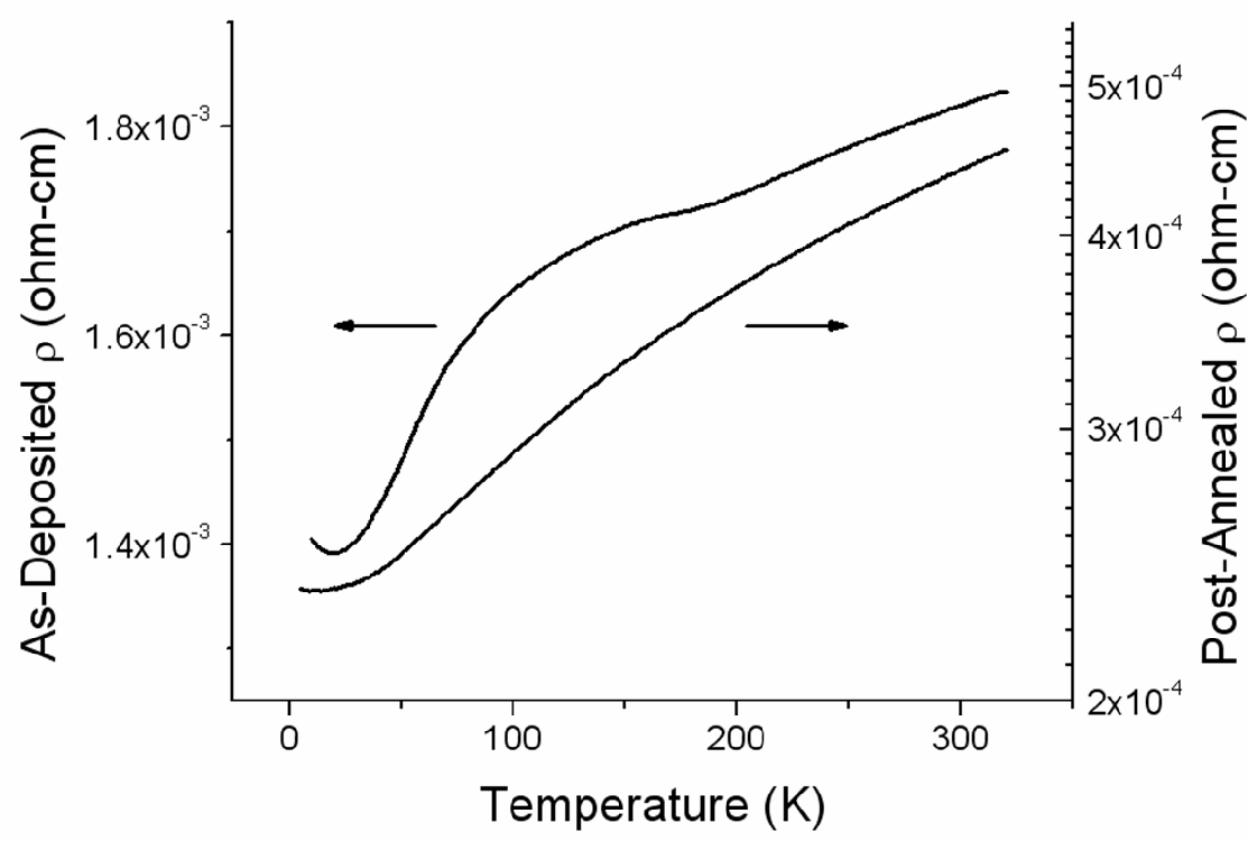
As-Deposited ρ (ohm-cm)
1.8x10-3
1.6x10-3
1.4x10-3
Post-Annealed ρ (ohm-cm)
5x10-4
4x10-4
3x10-4
2x10-4
0
100
200
300
Temperature (K)

Figure 8:

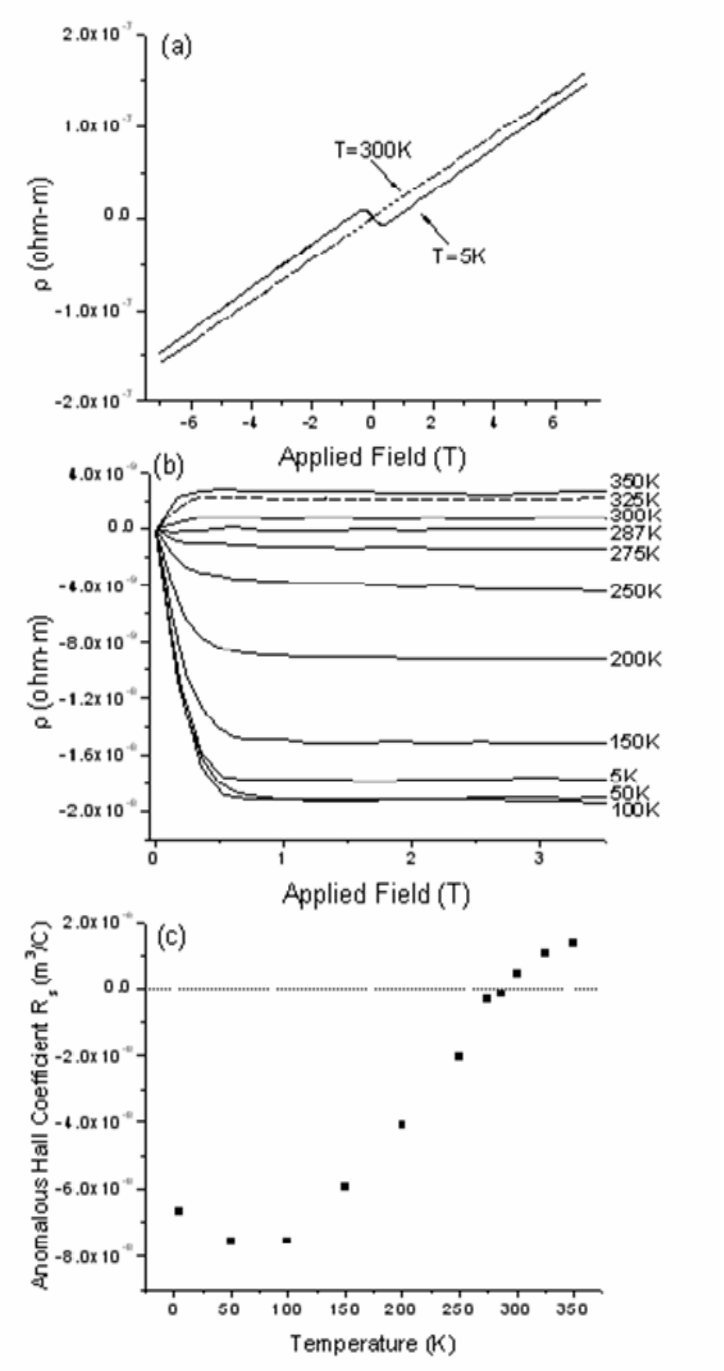
(a)
T=300K
T=5K
ρ (ohm-m)
Applied Field (T)
(b)
350K
325K
300K
287K
275K
250K
200K
150K
5K
50K
100K
ρ (ohm-m)
Applied Field (T)
(c)
Anomalous Hall Coefficient R_s (m^3/C)
Temperature (K)

Figure 9:

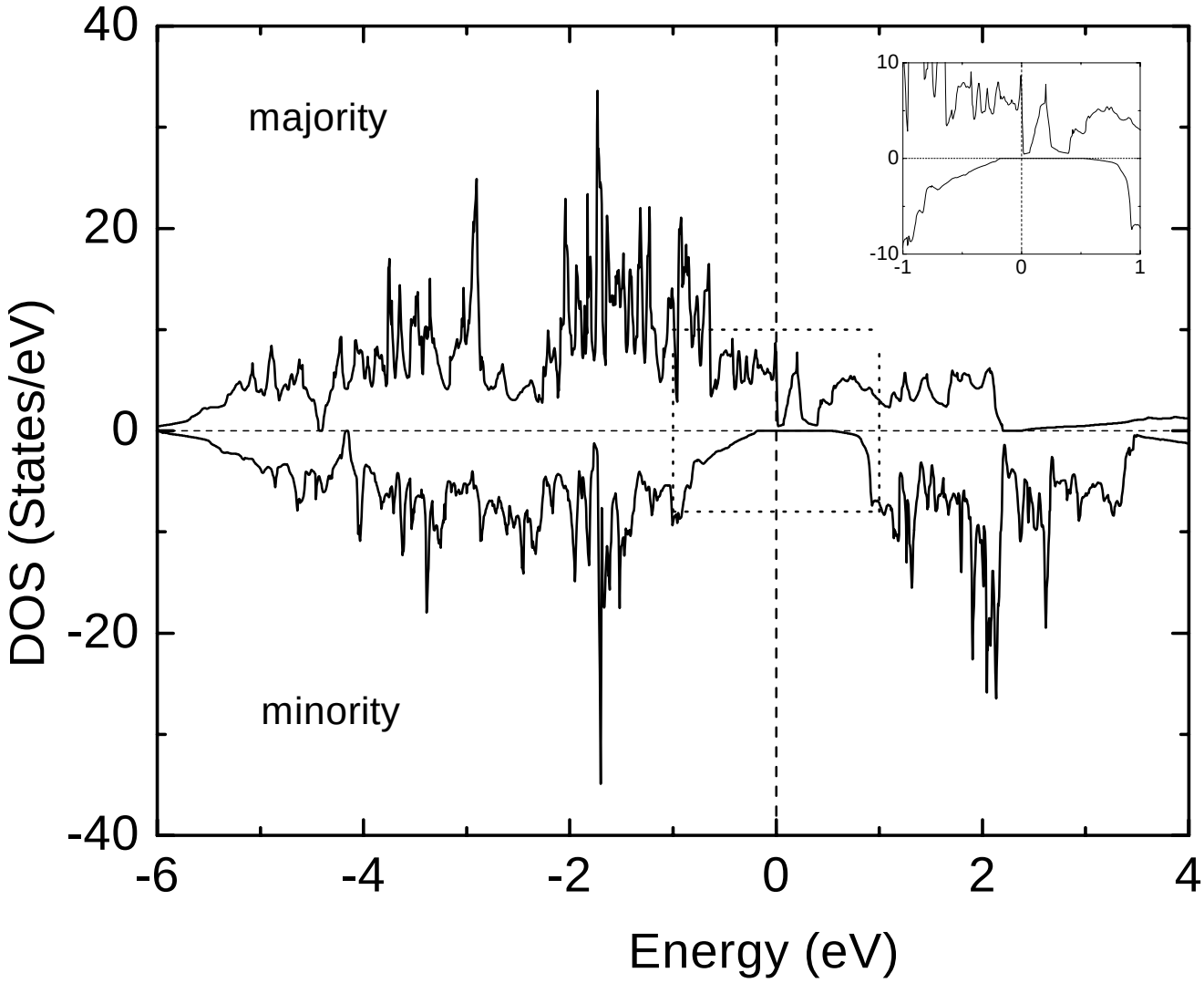
40
20
0
-20
-40
-6
-4
-2
0
2
4
DOS (States/eV)
Energy (eV)
majority
minority
10
0
-10
-1
0
1

Figure 10:

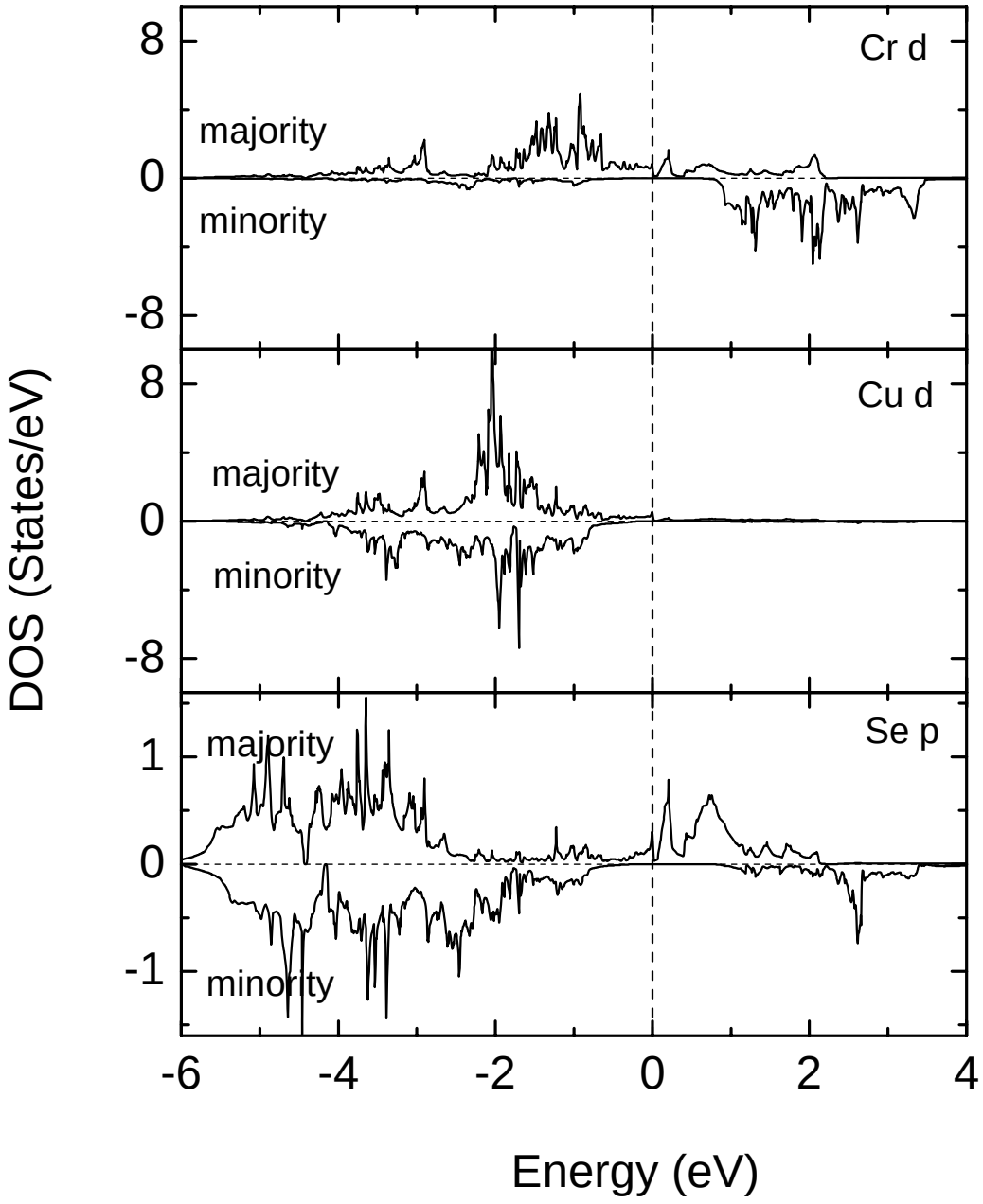
Cr d
majority
minority
Cu d
majority
minority
Se p
majority
minority
DOS (States/eV)
Energy (eV)
8
0
-8
8
0
-8
1
0
-1
-6
-4
-2
0
2
4

Figure 11:

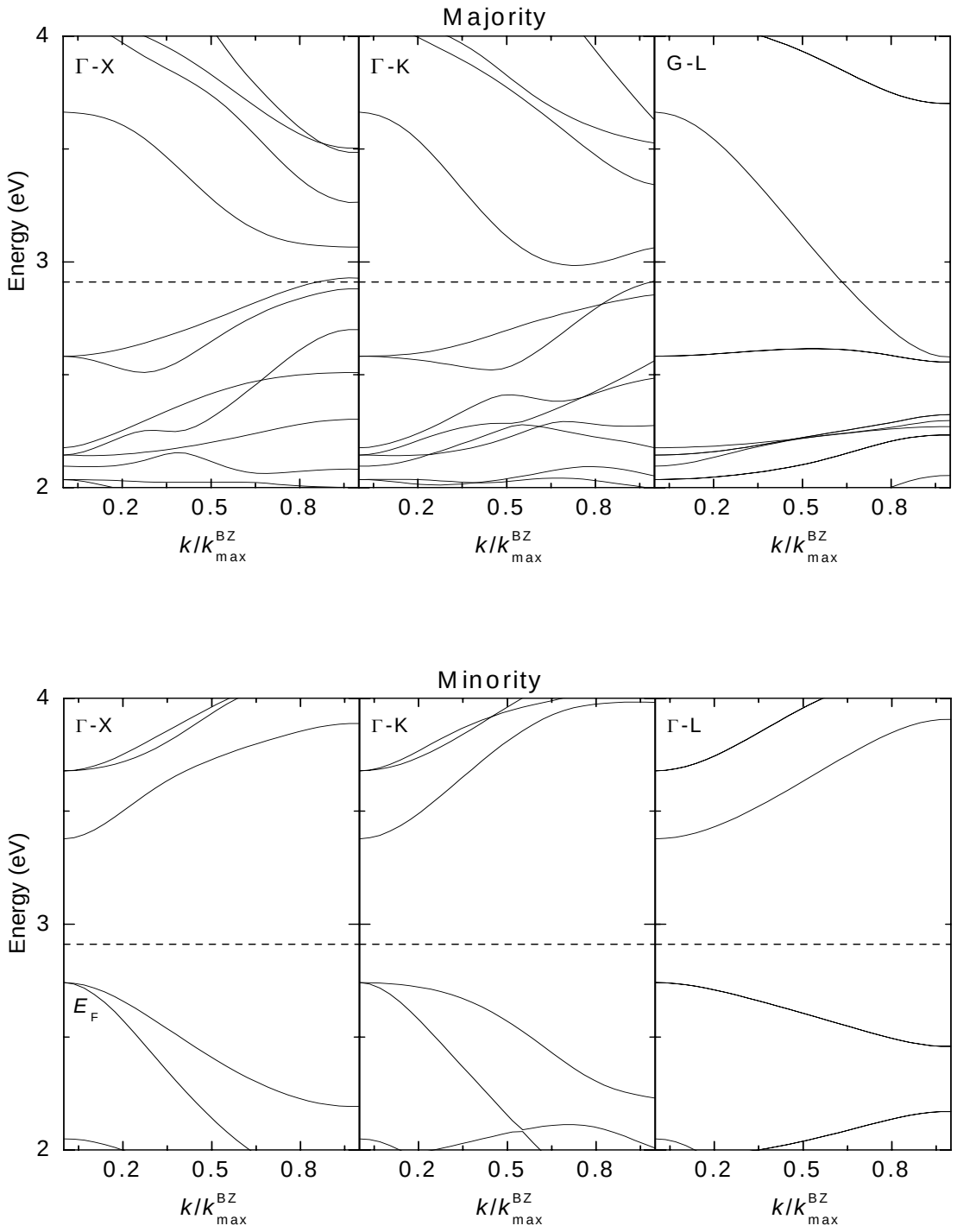
Majority
Γ-X
Γ-K
G-L
Energy (eV)
4
3
2
0.2
0.5
0.8
k/k^{BZ}_{max}
Minority
Γ-X
Γ-K
Γ-L
E_F